Chemical Science

ROYAL SOCIETY OF CHEMISTRY

EDGE ARTICLE

View Article Online
View Journal | View Issue

Cite this: *Chem. Sci.*, 2025, **16**, 20397

All publication charges for this article have been paid for by the Royal Society of Chemistry

Highly efficient and negligible efficiency roll-off non-doped blue electroluminescence with a synergistic effect of fast-balanced carrier transport and appropriate hybridized excited states

Huayi Zhou,[a] Tengyue Li,[a] Mizhen Sun,[b] Yannan Zhou,[a] Jingru Song,[a] Jie Zhang,[a] Qikun Sun,[a] Shi-Tong Zhang,[c] Xingrong Zhang *[a] and Shanfeng Xue *[a]

The most critical scientific problem for efficient blue emitters is to solve the inherent contradiction between wide bandgap characteristics and difficult carrier injection/unbalanced transmission. Herein, three donor–π–acceptor (D–π–A) type blue materials (TPACFTAZ, 9PCZCFTAZ, and 3PCZCFTAZ) based on fluorene-bridged and triazine acceptors were designed and synthesized. By regulating the donor strength and substitution sites, the synergistic optimization of solid-state aggregation mode and excited state characteristics has been achieved. Single crystal analysis shows that 3PCZCFTAZ exhibits the most abundant and effective intermolecular forces, obtaining fast-balanced carrier transport with electron and hole transport rates of 10.60×10^{-5} cm^2 V^{-1} s^{-1} and 9.53×10^{-5} cm^2 V^{-1} s^{-1}, respectively. Moreover, 3PCZCFTAZ also accomplished sufficient and stable hybridization between localized excited (LE) and charge transfer (CT) states, with a solid-state photoluminescence quantum yield (PLQY) of 71.2% and exciton utilization efficiency (EUE) of 82.2%. More importantly, the non-doped device based on 3PCZCFTAZ achieved a high EQE of 11.7%, with an efficiency roll-off of 0 @1000 cd m^{-2}. Among similar non-doped devices, this device exhibits not only negligible efficiency roll-off at high brightness, but also ranks among the most efficient reported to date.

Received 29th July 2025
Accepted 25th September 2025

DOI: 10.1039/d5sc05674h

rsc.li/chemical-science

Introduction

Blue electroluminescent materials play an irreplaceable role in expanding the display color gamut and achieving white light emission; therefore, the development of efficient and highly stable blue emitters is of paramount importance.[1–7] However, the wide bandgap characteristics of blue materials can cause difficulties in carrier injection and unbalanced transmission, which is the fundamental contradiction that makes it difficult to improve the efficiency of blue non-doped devices.[8–10] At present, the solution strategy for this problem mainly focuses on constructing two types of blue light molecular material systems: those based on the thermally activated delayed fluorescence (TADF) mechanism and those based on the hybrid localized charge transfer (HLCT) mechanism.[11–13] Traditional TADF blue materials usually have strong donor and acceptor abilities, which can improve the carrier transport capability while causing strong charge transfer (CT) excited states, resulting in severe spectral red-shift, so it is not conducive to the realization of blue light emission. And the utilization of triplet excitons in the TADF mechanism occurs between the lowest excited states ($T_1 \rightarrow S_1$), which can easily lead to the accumulation of triplet excitons and result in a significant efficiency roll-off.[14–16] Cheng *et al.* reported a TADF molecule 2DPyM-mDTC, it has a high efficiency (EQE) of up to 12.8% in the doped device, but its emission peak is located at 506 nm, and the efficiency roll-off is as high as 85% @500 cd m^{-2}.[17] Su *et al.* designed and synthesized multiple TADF molecules, among which the electroluminescence peaks (λ_{EL}) of molecules i-DMAc-TRZ and i-DMAc-BP were located at 450 nm and 465 nm, respectively, and the corresponding doped devices exhibited EQEs as high as 10.9% and 8.9%, respectively, but they also had high efficiency roll-offs of up to 90% and 71% @1000 cd m^{-2}, respectively.[18] In contrast, blue materials based on the HLCT mechanism have mild donors and acceptors, with localized excited (LE) and CT characteristics distributed in a certain proportion within their molecules.[19–23] These materials are expected to achieve high PLQY and EUE simultaneously.

[a]*State Key Laboratory of Advanced Optical Polymer and Manufacturing Technology, Key Laboratory of Rubber-Plastics of the Ministry of Education, Qingdao University of Science and Technology, 53-Zhengzhou Road, Qingdao 266042, P. R. China. E-mail: zhxr1984@126.com; sfxue@qust.edu.cn*

[b]*Shandong Engineering Research Center of Green and High-value Marine Fine Chemical, Shandong Peninsula Blue Economy and Engineering Research Institute, Weifang University of Science and Technology, Shouguang 262700, P. R. China*

[c]*State Key Laboratory of Supramolecular Structure and Materials, Institute of Theoretical Chemistry, College of Chemistry, Jilin University, Changchun 130012, P. R. China*

Furthermore, the utilization of triplet excitons occurs at high energy levels, and the fast and efficient exciton conversion can alleviate the serious efficiency roll-off problem.[24–27] Tang *et al.* reported a novel HLCT blue molecule CAT, featuring a high EQE of up to 10.39% in a non-doped device. It exhibited a blue emission with λ_{EL} at 441 nm, and has a low efficiency roll-off of only 21% @1000 cd m^{-2}.[26] Lu *et al.* constructed two newly HLCT type blue molecules, named PIAnTP and PyIAnTP, respectively. Both of them exhibited high performance in non-doped devices with EQE values of 8.36% and 8.69%, respectively. The λ_{EL} peaks were located at 456 nm and 464 nm, corresponding to deep-blue emission, with efficiency roll-offs of only 6% and 2% @1000 cd m^{-2}, respectively.[28] Although blue molecules based on the HLCT mechanism have shown relatively impressive performance, blue materials with EQE exceeding 11% and having negligible efficiency roll-off in non-doped devices are still rare. Therefore, it is particularly important to design novel, efficient and stable blue materials based on the HLCT mechanism.

In this work, with fluorene as the conjugated π-bridge and triazine as the acceptor, three novel HLCT emitters, TPACFTAZ, 9PCZCFTAZ and 3PCZCFTAZ, have been successfully developed. By changing the donor type and bonding site, effective regulation of the molecular stacking and the hybridization ratio of the LE/CT is achieved. Through single crystal analysis, it was found that 3PCZCFTAZ has the most abundant and optimum intermolecular forces in the solid state, which is very conducive to the transport of charge carriers. The test results also confirmed this point, 3PCZCFTAZ achieved fast-balanced carrier transport, with electron and hole transporting mobilities of 10.60×10^{-5} cm^2 V^{-1} s^{-1} and 9.53×10^{-5} cm^2 V^{-1} s^{-1}, respectively. In addition, the combination of photophysical testing and theoretical calculations indicates that 3PCZCFTAZ exhibits sufficiently hybridized LE/CT components, achieving a high PLQY and EUE of 71.2% and 82.2%, respectively. As a result, non-doped blue OLEDs fabricated with 3PCZCFTAZ achieved a high EQE of 11.7% along with zero efficiency roll-off at 1000 cd m^{-2}, representing some of the most efficient and stable blue OLEDs reported so far.

Results and discussion

Synthesis and molecular design

The molecular structures and synthetic routes of TPACFTAZ, 9PCZCFTAZ and 3PCZCFTAZ are shown in Scheme 1 and Scheme S1. Fluorene is a commonly used π-bridge because of its wide band gap and large conjugation planes, which are favorable for constructing blue emitting materials with multi-molecular intermolecular stacking. Meanwhile, in order to avoid serious aggregation-caused quenching (ACQ) caused by excessive stacking, 2,7-dibromo-9,9-di(1-propyl)-9*H*-fluorene with alkyl chains was used as the conjugated π-bridges. Triazine is a commonly used building block for electron transport materials, and its use as an acceptor can effectively enhance the electron transport and injection capabilities of the materials. First, triphenylamine (TPA) with propeller configuration was selected as the strong electron donating group, and the

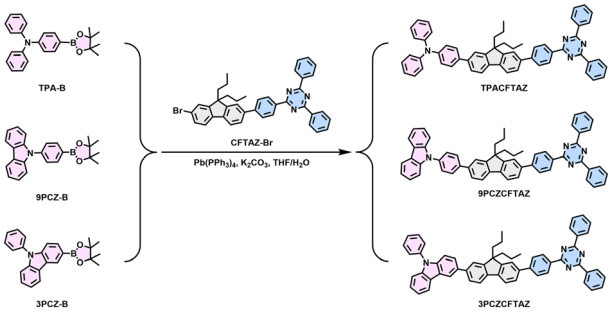

Scheme 1 Synthetic procedure and chemical structures of TPACFTAZ, 9PCZCFTAZ and 3PCZCFTAZ.

molecular TPACFTAZ was designed and successfully synthesized. Subsequently, in order to achieve precise control of the solid-state aggregation mode and excited state properties of molecules, 9-phenylcarbazole with higher planarity and weaker electron donating ability was introduced as the donor unit, and the molecule 9PCZCFTAZ was designed and prepared. In addition, by changing the bonding sites of phenylcarbazole, further synergistic optimization was carried out on the solid-state stacking and excited state characteristics of the molecule, and finally the molecule 3PCZCFTAZ was successfully obtained. All three compounds were synthesized by Suzuki coupling reaction and the final product yields were more than 80%, which were verified by ^1H, ^{13}C NMR, and mass spectrometry (Fig. S3–S11, SI). The experimental procedures describe the synthesis process and characterization data in detail.

Thermal and electrochemical properties

Thermal properties are a prerequisite for evaluating whether a material can be vacuum-deposited and used. In this regard, the thermal properties of the materials were tested using thermogravimetric analysis (TGA) and differential scanning calorimetry (DSC). As shown in Fig. S12 and Table S1, TPACFTAZ, 9PCZCFTAZ, and 3PCZCFTAZ all exhibited thermal decomposition temperatures (T_d) above 400 °C and glass transition temperatures (T_g) above 120 °C, indicating that they possessed good thermal stability and morphological stability in thin films. The redox behavior and electrochemical stability of the three materials were studied by cyclic voltammetry, and the results are shown in Fig. S13 and Table S1. All materials exhibited reversible redox peaks, and hence were electrochemically stable. The HOMO energy levels were −5.15 eV, −5.48 eV, and −5.41 eV, and the LUMO energy levels were −2.65 eV, −2.77 eV, and −2.79 eV for TPACFTAZ, 9PCZCFTAZ, and 3PCZCFTAZ, respectively. In addition, the corresponding HOMO–LUMO energy level gaps (E_g) are 2.50 eV, 2.71 eV and 2.62 eV respectively.

Theoretical calculations

The electronic properties of the target compounds were preliminarily evaluated through quantum chemical calculations.[29,30] Fig. 1(a) shows the ground state optimized configurations of the three compounds. Among the three compounds,

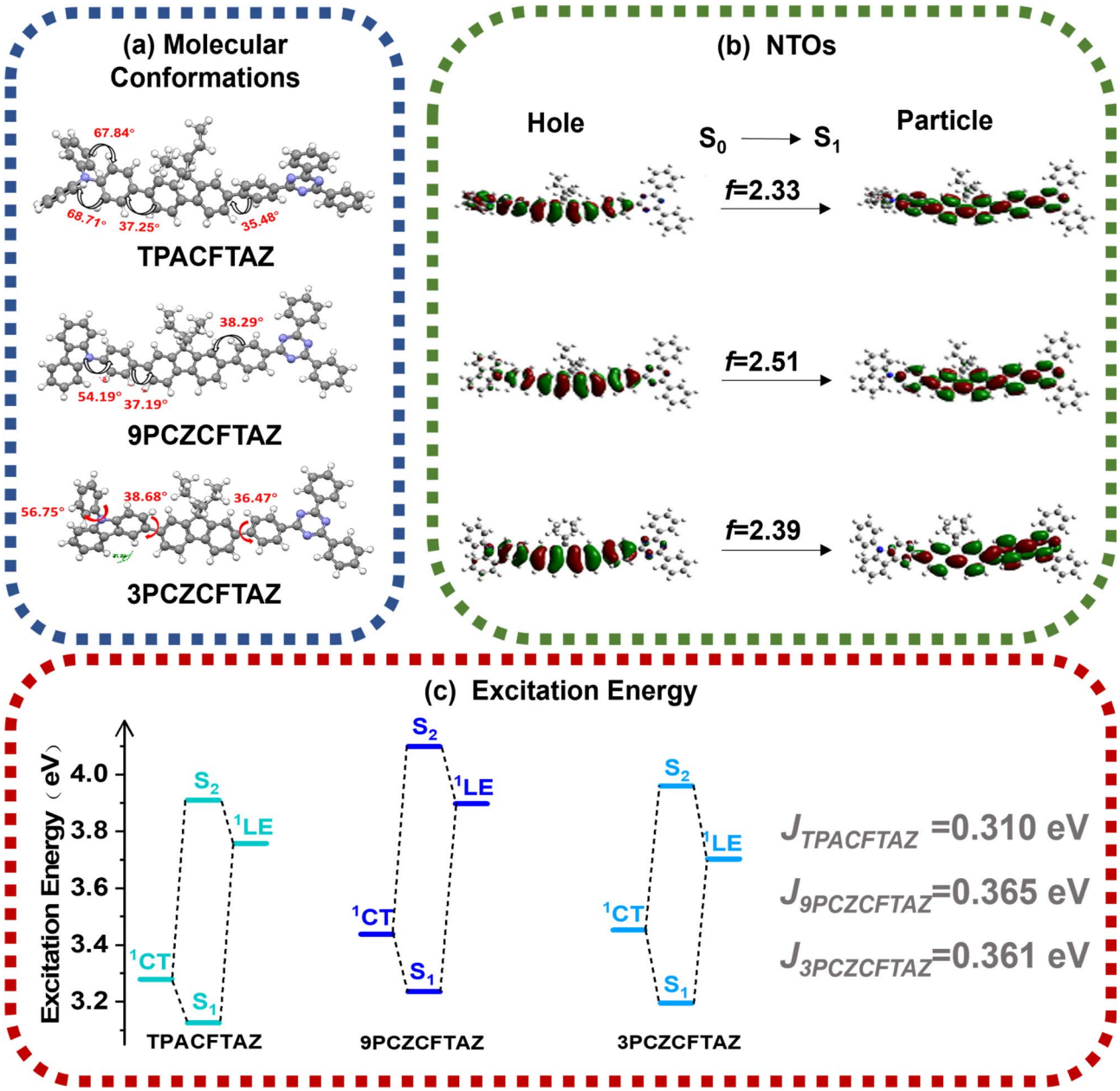

Fig. 1 (a) The geometries and structural formulae. (b) The $S_0 \rightarrow S_1$ natural transition orbitals (NTOs). (c) Energy diagram of state hybridization of the three compounds. Here, *J* refers to interstate coupling energy.

the fluorene plane with the aromatic ring bonded at its 2,7 position has a small torsion of less than 40°, and the torsion angle inside the acceptor triazine is only 20°, therefore, the difference in the degree of torsion of the three compounds is mainly determined by the donor. For TPACFTAZ, due to the unique propeller configuration of TPA, the two benzene rings at the end have large torsion angles of 68.71° and 67.84° with the fluorene-bonded benzene ring; for 9PCZCFTAZ, there is a torsion angle of 54.19° between carbazole and fluorene-bonded benzene rings; with the adjustment of the bonding position, the carbazole moiety of 3PCZCFTAZ is bonded directly to fluorene and has a torsion angle of only 38.68° with the fluorene; the end benzene ring has a 56.75° twist angle with fluorene. 3PCZCFTAZ has maximum conjugation. After adjusting the bonding position, the carbazole group of 3PCZCFTAZ is bonded to fluorene directly and has a torsion angle of only 38.68° with fluorene, which prolongs the main-chain conjugation. The planarity of the three molecules gradually increases, and 3PCZCFTAZ shows the greatest degree of conjugation and increased planarity. Fig. S14 shows the frontier molecular orbitals (FMOs) of the target compounds and their energy levels, and the energy level trends are consistent with the results of electrochemical tests. The HOMO energy level of TPACFTAZ is the shallowest (−4.90 eV), indicating that it is the strongest in electron-donation, which is associated with the strong electron-donating ability of trianiline; 9PCZCFTAZ has the deepest

HOMO energy level (−5.28 eV), indicating the weakest electron-donating ability; 3PCZCFTAZ has a slightly shallower HOMO energy level (−5.14 eV) than that of 9PCZCFTAZ, which corresponds to a slightly stronger electron-donating ability. Changing the bonding position can indeed change the donor strength and further change the excited state of the molecule. These are consistent with the original molecular design concept. Meanwhile, the natural transition orbitals (NTOs) of the lowest singlet excited state (S_1) were analyzed.

In Fig. 1(b), the hole and particle distributions of all three compounds show both overlapping and separated features, indicating that they have both LE and CT excited states. Due to the presence of LE states, TPACFTAZ, 9PCZCFTAZ, and 3PCZCFTAZ all exhibit large oscillator strengths (f) of 2.33, 2.51, and 2.39, respectively. Among them, 3PCZCFTAZ has a moderate value, indicating a moderate proportion of LE states.

Interstate coupling (J) represents the exciton coupling energy between the purely LE state and the purely CT state, serving as a key physical parameter that determines the formation of the HLCT state and the extent of its hybridization.[21,31–33] The interstate J of the three compounds was calculated from the energy of state hybridization shown in Fig. 1(c). Among them, the J values of 9PCZCFTAZ and 3PCZCFTAZ are relatively high, approximately above 0.360 eV, indicating that more sufficient and stable hybridization between LE and CT can be achieved. Fig. S15 shows the excited state energy levels in the first 10 singlet (S_1–S_{10}) and triplet (T_1–T_{10}) states of the molecule, and the three emitters have a T_1 and S_1 energy gap (ΔE_{ST}) of greater than 0.70 eV, suggesting a difficult $T_1 \rightarrow S_1$ process and hence a difficult TADF mechanism. Further, the energy gap between T_5 and S_1 of TPACFTAZ is less than 0.01 eV, between T_7 and S_1 of 9PCZCFTAZ is less than 0.01 eV, and between T_6 and S_1 of 3PCZCFTAZ is less than 0.03 eV. This suggests the existence of a potential thermal exciton channel between the single and trilinear states of each compound, allowing high-level triplet excitons to be utilized by converting them into singlet excitons through the reverse intersystem crossing (RISC) process.[34] In addition to theoretical simulations, the actual impact of distortions on molecular photophysics must be verified through experiments.

Photophysical properties

In order to fully study the photophysical properties of these three molecules, ultraviolet-visible (UV-vis) absorption spectroscopy (Fig. S16) and photoluminescence (PL) spectroscopy tests were performed in different polar solvents and thin films, respectively. As shown in Fig. 2(a), the target compounds exhibit a clear vibrational fine structure in hexane, which suggests that the S_1 state of the three molecules is dominated by the LE state at low polarity. As the solvent polarity increases, the spectra exhibit the disappearance of the vibrational fine structure, spectral broadening and a gradual redshift, which suggests the dominance of the CT state in high polarity solutions. During the transition process, hybridization between LE and CT occurs, which is one of the typical characteristics of the HLCT state. And transitioning from *n*-hexane to dichloromethane, the emission peaks of TPACFTAZ, 9PCZCFTAZ, and 3PCZCFTAZ exhibited red shifts of 144 nm, 62 nm, and 91 nm, respectively. The CT state of TPACFTAZ is the strongest, 9PCZCFTAZ is the weakest, and 3PCZCFTAZ has the most moderate CT state, which is related to its electron donating ability and consistent with theoretical calculations. In addition, the PLQYs of the three compounds were tested in different polar solvents and films as shown in Table 1. In the neat film, TPACFTAZ has the smallest PLQY due to the strong CT state properties, which leads to a sharp decrease in PLQY to 27.2%. In contrast, 9PCZCFTAZ and 3PCZCFTAZ exhibit excellent PLQYs of 70.3% and 71.2%, respectively. It is noteworthy that 3PCZCFTAZ maintains a high PLQY while the contribution of the CT state is enhanced, and it is speculated that it has achieved an effective balance of the

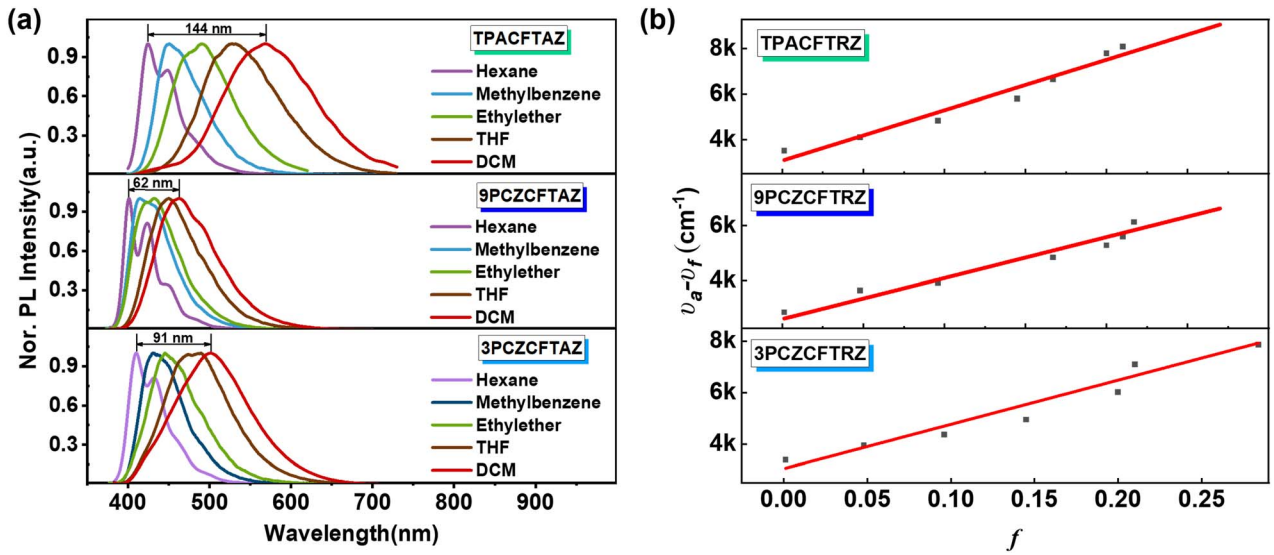

Fig. 2 TPACFTAZ, 9PCZCFTAZ and 3PCZCFTAZ of (a) Normalized PL spectra in different solvents with increasing polarity; (b) Stokes shift curves.

Table 1 Photophysical properties of the three compounds

	λ_{PL}[a] (nm)				φ_{PL}[b] (%)		τ[c] (ns)	
Molecules	Hexane	THF	DCM	Film	THF	Film	THF	Film
TPACFTAZ	424	528	568	492	79.1	27.7	3.57	4.08
9PCZCFTAZ	401	450	463	450	95.3	70.3	1.48	4.85
3PCZCFTAZ	410	489	501	459	97.6	71.2	2.64	6.28

[a] λ_{PL}: Maximum emission wavelength, concentration: 10^{-5} M. [b] Φ_{PL}: Absolute fluorescence quantum efficiency. [c] τ: Fluorescence lifetime.

excited state components by rationally regulating the hybridisation ratio between the LE state and the CT state. The stokes shift curves (Fig. 2(b)) derived from the solvatochromic results show that the data for all three compounds could be fitted with a monophasic model. This observation further supports that the locally excited (LE) and charge-transfer (CT) states exhibit sufficient hybridization. The transient photoluminescence (PL) decay spectra of the compounds in both solution and ordered thin films (Fig. S18) display single-exponential decay characteristic on the nanosecond timescale, confirming that all emitters arise from a non-delayed fluorescence process originating from a single excited state, the result which excludes the possibility of the TADF mechanism. Furthermore, fluorescence/phosphorescence spectra were measured at 77 K (Fig. S19). The S_1 energies (E_{S1}) for TPACFTAZ, 9PCZCFTAZ, and 3PCZCFTAZ were determined to be 2.75 eV, 2.99 eV, and 2.88 eV, respectively, while the T_1 energies (E_{T_1}) were found to be 2.33 eV, 2.30 eV, and 2.37 eV, respectively. The corresponding experimental ΔE_{ST} values are 0.76 eV, 0.85 eV, and 0.83 eV. These large ΔE_{ST} values hinder the RISC process from T_1 to S_1, thereby precluding the occurrence of the TADF mechanism in these materials.

Carrier transport properties

To investigate the influence of molecular design and functional group modulation on charge carrier mobilities, we fabricated single-electron devices with the structure ITO/LiF (1 nm)/TPBi (10 nm)/EMLs (80 nm)/LiF (1 nm)/Al (100 nm) and single-hole devices with the structure ITO/HATCN (20 nm)/EMLs (80 nm)/HATCN (20 nm)/Al (100 nm). The corresponding results are summarized in Fig. 3 and Table S2. The electron mobility (μ_{ele}) and hole mobility (μ_h) of each material are in the same order of magnitude, indicating an appropriate match in the selection of donor/acceptor moieties. In organic material systems, μ_h is usually higher than μ_{ele}, while the materials in this study exhibit slightly higher μ_{ele} than μ_h, which will simplify the design of device structures. In addition, under an electric field of 10^5 V cm^{-1}, the carrier mobility of the three compounds is on the order of 10^{-5} cm^2 V^{-1} s^{-1}, which is related to the excellent electron transport ability of triazine acceptors. Among them, by modulating the functional group bonding sites, 3PCZCFTAZ achieved fast-balanced mobilities, with μ_h and μ_{ele} reaching 9.53×10^{-5} cm^2 V^{-1} s^{-1} and 10.60×10^{-5} cm^2 V^{-1} s^{-1}, respectively.

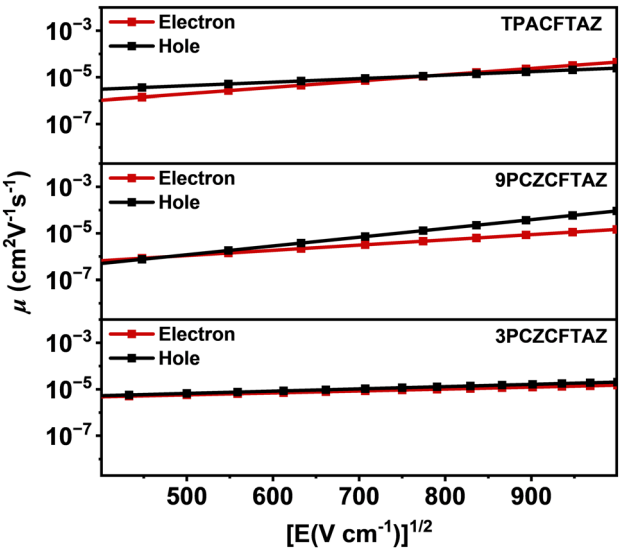

Fig. 3 Carrier mobility curves of TPACFTAZ, 9PCZCFTAZ and 3PCZCFTAZ.

Single-crystal structure

The stacking pattern and distance between multimolecules determine the carrier mobility level of the compounds.[35–37] In order to investigate the mechanism of the effect of the modulation of the bonding site of the donor group on the mobility, we prepared single crystals of 9PCZCFTAZ and 3PCZCFTAZ by vacuum sublimation and analysed their stacking structures. The single-crystal structure reveals the intrinsic molecular packing characteristics of the material. This inherent packing propensity induces the formation of analogous charge transport pathways within localized regions of its amorphous thin films, thereby providing crucial insight into the material's electron transporting behavior. Single-molecule conformational analysis (Fig. 4(a)) showed that the actual torsion angle of the carbazole moiety of 9PCZCFTAZ was significantly larger than the theoretically calculated value, implying that this moiety triggers stronger intermolecular steric hindrance in the solid state. Fig. 4(b) shows the multimolecular intermolecular stacking, and both compounds have regular molecular arrangement and abundant weak intermolecular interactions. First, 9PCZCFTAZ has a one-dimensional lamellar stacking structure with abundant weak intermolecular C–H$\cdots\pi$ (3.07–3.70 Å) and C–H$\cdots$N (3.31–3.64 Å) interactions. The neighbouring molecules are arranged face-to-face with alternating phenylcarbazole (D) and triazine (A) groups, and this D/A alternating stacking pattern is conducive to balanced electron/hole transport. It is worth noting that the carbazole group of 9PCZCFTAZ has a larger twist angle with the main chain of the molecule, so there are fewer intermolecular interactions on the donor, which may be the structural reason for its μ_h being lower than μ_{ele}. 3PCZCFTAZ reduces the torsion angle of the carbazole–fluorene plane by optimizing the donor bonding site, and the reduction of conjugate extension and steric hindrance induces the formation of an uninterrupted two-dimensional lamellar stacking

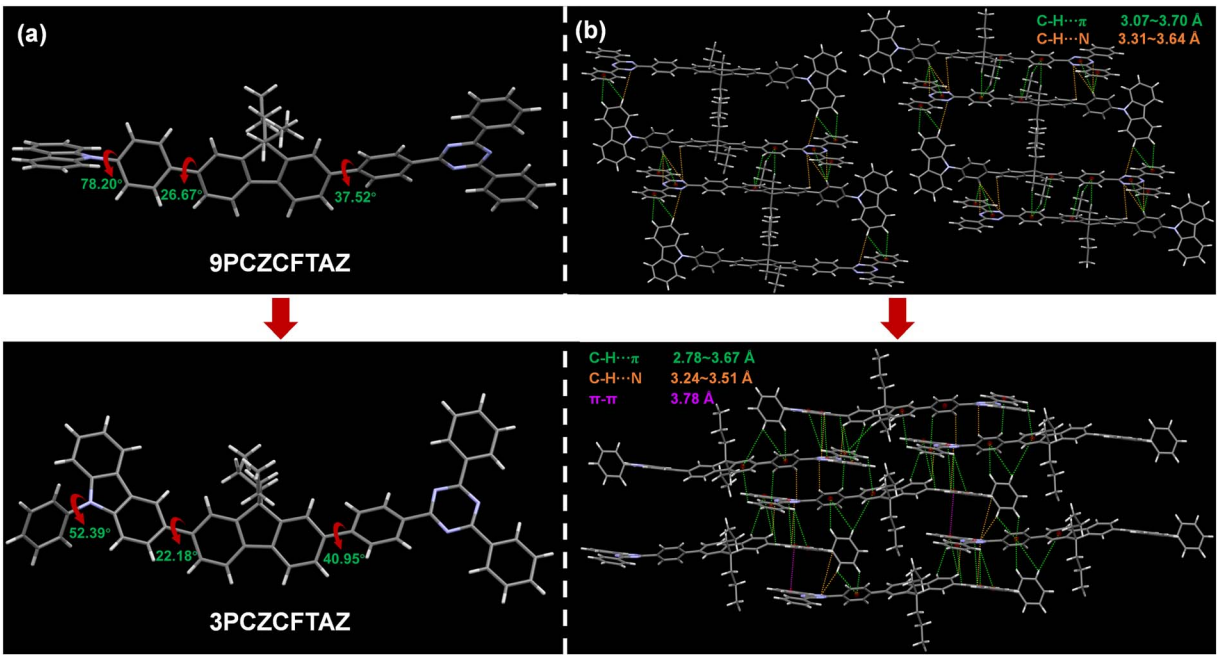

Fig. 4 9PCZCFTAZ and 3PCZCFTAZ in (a) molecular configuration in the crystalline state; (b) solid state stacking method and intermolecular interactions.

structure between its molecules, so that the weak intermolecular interactions are stronger and richer, with C–H···π (2.78–3.67 Å), C–H···N (3.24–3.51 Å) and weak π–π (3.78 Å) interactions. This two-dimensional laminar stacking is considered to be the most efficient for charge transport, as it allows the transport of charge carriers by almost straight lines.[38–41] The arrangement between adjacent molecules mainly presents a tight D–A face-to-face alternating stacking, and therefore, the mobility of both electrons and holes is high. In addition, weak A–A stacking is observed, so that the μ_{ele} of the molecule is understandably slightly higher than the μ_h. The above results indicate that precise tuning of the stacking dimension and interaction strength is the key to obtaining fast-balanced mobility, which provides a structural basis for the subsequent design of high-performance devices.

Electroluminescence performance

On the basis of the HOMO/LUMO energy levels and carrier mobility properties of the three materials, we have fabricated non-doped electroluminescent devices with a simple structure: ITO/PEDOT : PSS (40 nm)/TCTA (15 nm)/emitters (20 nm)/TPBi (35 nm)/LiF (1 nm)/Al (100 nm), where poly(2, 3-dihydrothiophene-1, 4-dioxin)-poly(styrene sulfonate) (PEDOT : PSS) is the hole injection layer, tris(4-(9*H*-carbazol-9-yl) phenyl) amine (TCTA) is the hole transport and electron blocking layer, 1,3,5-tri(phenyl-2-benzimidazolyl)benzene (TPBi) is the electron transport layer while also functioning as the hole blocking layer, LiF is the electron injection layer, and Al is the cathode. The non-doped devices with TPACFTAZ, 9PCZCFTAZ and 3PCZCFTAZ as electroluminescent layers (EMLs) are named B1, B2 and B3, respectively, and their device energy levels are shown in Fig. S21, and the electroluminescence (EL) performances are summarized in Fig. 5 and Table S2. The EL emission peaks of B1, B2, and B3 were observed at 487 nm, 456 nm and 460 nm, with corresponding CIE coordinates of (0.18, 0.35), (0.15, 0.15) and (0.16, 0.18), respectively, achieving color tuning from sky-blue to pure-blue emission. Notably, the EL spectra closely matched the PL spectra of the corresponding neat films, indicating that the electron and hole mobilities were balanced within the devices, the emitting region was successfully confined to the EML, and the device structures were well-designed. Further, all three devices have low turn-on voltages, and the EL spectra of the three devices were almost unchanged at different operating voltages (Fig. S22), indicating that the injection of electrons and holes into the devices is relatively easy, and the transmission rate varies equally at different voltages, indicating that the transmission process is relatively stable. B1, B2 and B3 achieved EQE_{max} up to 5.0%, 9.7% and 11.7%, respectively. The maximum current efficiency (CE_{max}) and maximum power efficiency (PE_{max}) are 11.0, 12.6, and 18.6 cd A^{-1}, and 9.1, 8.0, and 14.3 lm W^{-1}, respectively. B3 achieved the highest device efficiency, and it possesses 0 roll-off at 1000 cdm^{-2} for the non-doped device, thanks to its excellent solid-state stacking mode and optimal LE/CT hybridization ratio. Fig. 6 and Table S3 summarize the performance of non-doped blue devices based on the HLCT mechanism published in recent years. It can be seen that the 3PCZCFTAZ device not only achieves the highest stability, but also ranks among the most efficient ones. According to the EQE obtained from the test, the EUEs of the three were calculated to be 90.3%, 69.7%, and 82.2%, respectively, which exhibit a positive correlation with the intensity of their CT states. It is worth noting that compared to

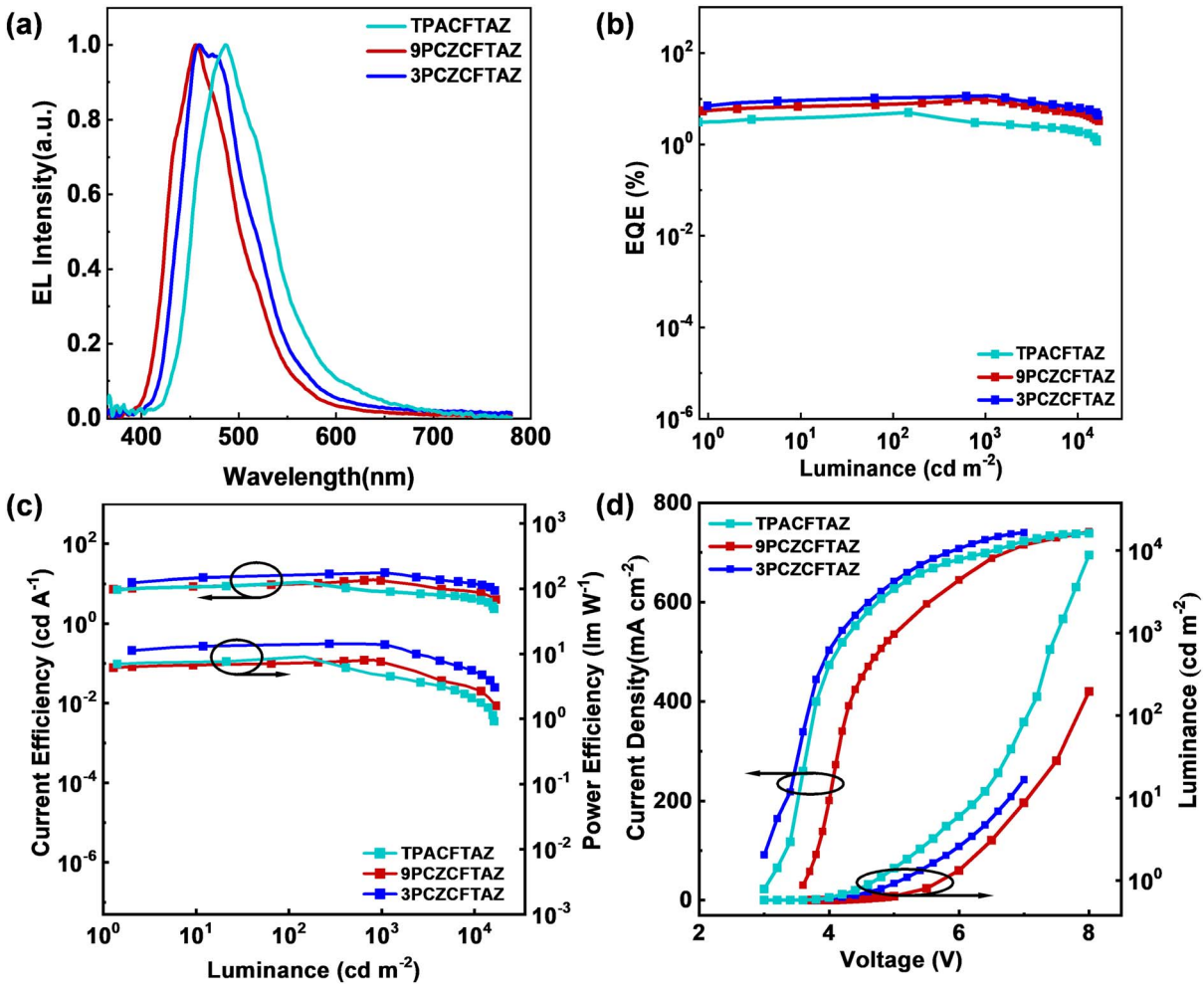

Fig. 5 Non-doped device performance based on three compounds. (a) EL spectra; (b) EQE–luminance curves; (c) current efficiency–luminance–power efficiency curves.; (d) current density–voltage–luminance curves.

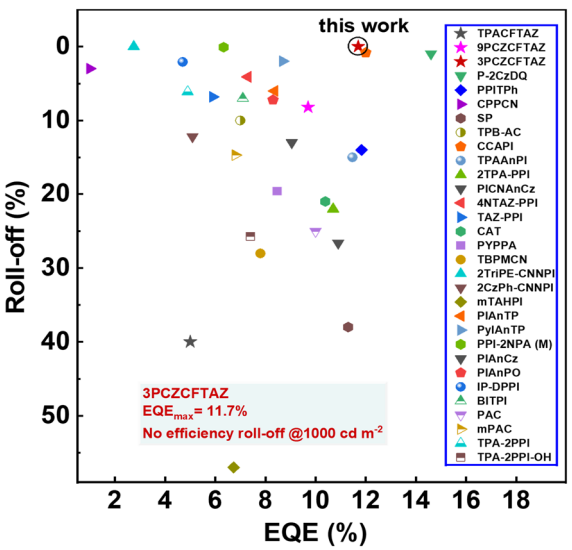

Fig. 6 Summary of non-doped blue devices based on the HLCT mechanism ($\lambda_{EL} \leq 470$ nm) published in recent years.

B2, B3 maintains almost unchanged emission wavelength by changing the donor bonding site and increasing the CT component ratio. However, the efficiency of the undoped device is improved by 20%, this indicates that small molecular regulation can greatly affect the optoelectronic properties of molecules, and the correct molecular bonding method can lead to remarkably improved performance.

Conclusions

In summary, three novel blue electroluminescent materials based on the triazine acceptor were designed and synthesized. By strategically modulating the donor units, conjugation length, and torsional configuration of the molecules, dual regulation of its solid-state aggregation mode and excited state characteristics has been achieved. Single crystal analysis shows that 3PCZCFTAZ has the richest and optimum intermolecular forces, and characterization of single-carrier devices further indicates that 3PCZCFTAZ exhibits fast-balanced carrier mobilities. The combination of photophysical analysis and theoretical calculations shows that the LE/CT hybridization

state of 3PCZCFTAZ has reached the optimal level, while obtaining 71.2% PLQY and 82.2% EUE. Benefiting from the optimized excited state distribution and balanced carrier transport properties, the 3PCZCFTAZ-based non-doped pure blue device achieves an EQE_{max} of 11.7% and maintains no efficiency roll-off @1000 cd m^{-2}. This study provides a reference strategy for designing efficient and stable blue emitters by achieving fast-balanced carrier mobilities.

Author contributions

T. Li and H. Zhou conducted the synthesis, characterization of basic properties, and fabrication and characterization studies of the devices. H. Zhou wrote the manuscript. M. Sun, J. Zhang, L. Zhang and Q. Sun reviewed and revised the manuscript. Y. Zhou supported the theoretical calculations. S. Xue and X. Zhang conceived the idea, supervised this study and revised this article.

Conflicts of interest

There are no conflicts to declare.

Data availability

CCDC 2358763, 2358764, 2358765, 2358766, 2358767, 2358768, 2358769, 2358770, 2358771, and 2358772 contain the supplementary crystallographic data for this paper.[42a–j]

The data supporting this article have been included as part of the SI. Supplementary Information: compound syntheses and characterization, other theoretical calculations, spectra, morphology of films and other device performances. See DOI: https://doi.org/10.1039/d5sc05674h.

Acknowledgements

This work was supported by the Natural Science Foundation of Shandong Province (No. ZR2025MS879); the National Natural Science Foundation of China (No. 51873095); the Taishan Scholar Constructive Engineering Foundation of Shandong Province of China (No. tsqn202211164); the Natural Science Foundation of Qingdao City of China (No. 23-2-1-239-zyyd-jch); and the Open Fund of the State Key Laboratory of Luminescent Materials and Devices, South China University of Technology (No. 2025-skllmd-10).

Notes and references

1 J. Zhao, B. Liu, Z. Wang, Q. Tong, X. Du, C. Zheng, H. Lin, S. Tao and X. Zhang, *ACS Appl. Mater. Interfaces*, 2018, **10**, 9629–9637.
2 K. Kreger, M. Bäte, C. Neuber, H. W. Schmidt and P. Strohriegl, *Adv. Funct. Mater.*, 2007, **17**, 3456–3461.
3 Y. Sun, N. C. Giebink, H. Kanno, B. Ma, M. E. Thompson and S. R. Forrest, *Nature*, 2006, **440**, 908–912.
4 C. J. Zheng, J. Wang, J. Ye, M. F. Lo, X. K. Liu, M. K. Fung, X. H. Zhang and C. S. Lee, *Adv. Mater.*, 2013, **25**, 2205–2211.
5 B. Chen, B. Liu, J. Zeng, H. Nie, Y. Xiong, J. Zou, H. Ning, Z. Wang, Z. Zhao and B. Z. Tang, *Adv. Funct. Mater.*, 2018, **28**, 1–12.
6 Y. Yu, P. Xu, Y. Pan, X. Qiao, L. Ying, D. Hu, D. Ma and Y. Ma, *Adv. Opt. Mater.*, 2023, **11**, 1–8.
7 P. I. Shih, C. Y. Chuang, C. H. Chien, E. W. G. Diau and C. F. Shu, *Adv. Funct. Mater.*, 2007, **17**, 3141–3146.
8 H. Liu, Q. Bai, L. Yao, H. Zhang, H. Xu, S. Zhang, W. Li, Y. Gao, J. Li, P. Lu, H. Wang, B. Yang and Y. Ma, *Chem. Sci.*, 2015, **6**, 3797–3804.
9 H. Yang, Q. Liang, C. Han, J. Zhang and H. Xu, *Adv. Mater.*, 2017, **29**, 1–9.
10 S. N. Zou, X. Chen, S. Y. Yang, S. Kumar, Y. K. Qu, Y. J. Yu, M. K. Fung, Z. Q. Jiang and L. S. Liao, *Adv. Opt. Mater.*, 2020, **8**, 1–7.
11 T. Liu, X. Chen, J. Zhao, W. Wei, Z. Mao, W. Wu, S. Jiao, Y. Liu, Z. Yang and Z. Chi, *Chem. Sci.*, 2021, **12**, 5171–5176.
12 X. Cai, B. Gao, X. L. Li, Y. Cao and S. J. Su, *Adv. Funct. Mater.*, 2016, **26**, 8042–8052.
13 Z. Zhong, X. Zhu, X. Wang, Y. Zheng, S. Geng, Z. Zhou, X. J. Feng, Z. Zhao and H. Lu, *Adv. Funct. Mater.*, 2022, **32**, 2112969.
14 M. Sun, R. Wang, C. Ma, Y. Zhou, X. Wang, L. Chu, W. Yang and S. Xue, *Chem. Eng. J.*, 2025, **507**, 160436.
15 Q. Zhang, J. Li, K. Shizu, S. Huang, S. Hirata, H. Miyazaki and C. Adachi, *J. Am. Chem. Soc.*, 2012, **134**, 14706–14709.
16 X. Tang, Q. Bai, Q. Peng, Y. Gao, J. Li, Y. Liu, L. Yao, P. Lu, B. Yang and Y. Ma, *Chem. Mater.*, 2015, **27**, 7050–7057.
17 P. Rajamalli, N. Senthilkumar, P. Y. Huang, C. C. Ren-Wu, H. W. Lin and C. H. Cheng, *J. Am. Chem. Soc.*, 2017, **139**, 10948–10951.
18 X. Cai, B. Gao, X. Li, Y. Cao and S. Su, *Adv. Funct. Mater.*, 2016, **26**, 8042–8052.
19 G. Li, B. Li, H. Zhang, X. Guo, C. Lin, K. Chen, Z. Wang, D. Ma and B. Z. Tang, *ACS Appl. Mater. Interfaces*, 2022, **14**, 10627–10636.
20 J. Yang, Q. Guo, J. Wang, Z. Ren, J. Chen, Q. Peng, D. Ma and Z. Li, *Adv. Opt. Mater.*, 2018, **6**, 1–8.
21 S. Zhang, L. Yao, Q. Peng, W. Li, Y. Pan, R. Xiao, Y. Gao, C. Gu, Z. Wang, P. Lu, F. Li, S. Su, B. Yang and Y. Ma, *Adv. Funct. Mater.*, 2015, **25**, 1755–1762.
22 H. Zhang, B. Zhang, Y. Zhang, Z. Xu, H. Wu, P. A. Yin, Z. Wang, Z. Zhao, D. Ma and B. Z. Tang, *Adv. Funct. Mater.*, 2020, **30**, 1–10.
23 C. Zhou, D. Cong, Y. Gao, H. Liu, J. Li, S. Zhang, Q. Su, Q. Wu and B. Yang, *J. Phys. Chem. C*, 2018, **122**, 18376–18382.
24 Z. Wang, Y. Feng, S. Zhang, Y. Gao, Z. Gao, Y. Chen, X. Zhang, P. Lu, B. Yang, P. Chen, Y. Ma and S. Liu, *Phys. Chem. Chem. Phys.*, 2014, **16**, 20772–20779.
25 W. Cui, C. Liu, X. Chao, M. Xie, Q. Sun, D. Liu, Y. Pan, S. T. Zhang, S. Xue and W. Yang, *Adv. Opt. Mater.*, 2023, **11**, 1–8.
26 B. Li, J. Lou, H. Zhang, G. Li, X. He, Y. Huang, N. Zheng, Z. Wang, D. Ma and B. Z. Tang, *Adv. Funct. Mater.*, 2023, **33**, 1–10.
27 C. Liao, B. Chen, Q. Xie, X. Li, H. Liu and S. Wang, *Adv. Mater.*, 2023, **35**, 1–12.

28 F. Liu, G. Cao, Z. Feng, Z. Cheng, Y. Yan, Y. Xu, Y. Jiang, Y. Chang, Y. Lv and P. Lu, *ACS Appl. Mater. Interfaces*, 2023, **15**, 47307–47316.
29 F. Neese, *Rev. Comput. Mol. Sci.*, 2018, **8**, 1–6.
30 F. Neese, *Wiley Interdiscip. Rev. Comput. Mol. Sci.*, 2022, **12**, 1–15.
31 S. F. Völker, A. Schmiedel, M. Holzapfel, K. Renziehausen, V. Engel and C. Lambert, *J. Phys. Chem. C*, 2014, **118**, 17467–17482.
32 C. Lambert, T. Scherpf, H. Ceymann, A. Schmiedel and M. Holzapfel, *J. Am. Chem. Soc.*, 2015, **137**, 3547–3557.
33 Y. Gao, S. Zhang, Y. Pan, L. Yao, H. Liu, Y. Guo, Q. Gu, B. Yang and Y. Ma, *Phys. Chem. Chem. Phys.*, 2016, **18**, 24176–24184.
34 H. Zhang, G. Li, X. Guo, K. Zhang, B. Zhang, X. Guo, Y. Li, J. Fan, Z. Wang, D. Ma and B. Z. Tang, *Angew. Chem., Int. Ed.*, 2021, **133**, 22415–22421.
35 K. Zhang, Z. Zhou, D. Liu, Y. Chen, S. Zhang, J. Pan, X. Qiao, D. Ma, S. J. Su, W. Zhu and Y. Liu, *Angew. Chem., Int. Ed.*, 2024, **63**, 202407502.
36 H. Zhou, R. Wang, M. Sun, Y. Zhou, L. Zhang, J. Song, Q. Sun, S.-T. Zhang, W. Yang and S. Xue, *Chem. Sci.*, 2024, **15**, 18601–18607.
37 H. Zhou, T. Li, M. Xie, Y. Zhou, Q. Sun, S.-T. Zhang, Y. Zhang, W. Yang and S. Xue, *Chem. Sci.*, 2024, **15**, 8106–8111.
38 J. E. Anthony, J. S. Brooks, D. L. Eaton and S. R. Parkin, *J. Am. Chem. Soc.*, 2001, **123**, 9482–9483.
39 C. Wang, H. Dong, H. Li, H. Zhao, Q. Meng and W. Hu, *Cryst. Growth Des.*, 2010, **10**, 4155–4160.
40 C. Wang, H. Dong, W. Hu, Y. Liu and D. Zhu, *Chem. Rev.*, 2012, **112**, 2208–2267.
41 H. Liu, Z. Xu, J. Zhang, L. Rao, Y. Ge, Z. Xia, X. Zhang, L. Jiang, Y. Yi, B. Yang and Y. Ma, *Adv. Mater.*, 2025, **37**, 2419981.
42 (*a*) CCDC 2358763, Experimental Crystal Structure Determination, 2025, DOI: **10.5517/ccdc.csd.cc2k5h4d**; (*b*) CCDC 2358764, Experimental Crystal Structure Determination, 2025, DOI: **10.5517/ccdc.csd.cc2k5h5f**; (*c*) CCDC 2358765, Experimental Crystal Structure Determination, 2025, DOI: **10.5517/ccdc.csd.cc2k5h6g**; (*d*) CCDC 2358766, Experimental Crystal Structure Determination, 2025, DOI: **10.5517/ccdc.csd.cc2k5h7h**; (*e*) CCDC 2358767, Experimental Crystal Structure Determination, 2025, DOI: **10.5517/ccdc.csd.cc2k5h8j**; (*f*) CCDC 2358768, Experimental Crystal Structure Determination, 2025, DOI: **10.5517/ccdc.csd.cc2k5h9k**; (*g*) CCDC 2358769, Experimental Crystal Structure Determination, 2025, DOI: **10.5517/ccdc.csd.cc2k5hbl**; (*h*) CCDC 2358770, Experimental Crystal Structure Determination, 2025, DOI: **10.5517/ccdc.csd.cc2k5hcm**; (*i*) CCDC 2358771, Experimental Crystal Structure Determination, 2025, DOI: **10.5517/ccdc.csd.cc2k5hdn**; (*j*) CCDC 2358772, Experimental Crystal Structure Determination, 2025, DOI: **10.5517/ccdc.csd.cc2k5hfp**.